REPORT 928

ANALYSIS OF PERFORMANCE OF JET ENGINE FROM CHARACTERISTICS OF COMPONENTS II—INTERACTION OF COMPONENTS AS DETERMINED FROM ENGINE OPERATION

By Arthur W. Goldstein, Sumner Alpert, William Beede, and Karl Kovach

SUMMARY

In order to understand the operation and the interaction of jet-engine components during engine operation and to determine how component characteristics may be used to compute engine performance, a method to analyze and to estimate performance of such engines was devised and applied to the study of the characteristics of a research turbojet engine built for this investigation. An attempt was made to correlate turbine performance obtained from engine experiments with that obtained by the simpler procedure of separately calibrating the turbine with cold air as a driving fluid in order to investigate the applicability of component calibration. After correction for blade-tip leakage, the turbine-characteristic curves of weight flow and total-pressure ratio checked with the results from cold-air component calibration. Some discrepancies in efficiency were noted between the two sets of experiments. Despite such errors, turbine-compressor interaction may be accurately determined but some error in exhaust pressure may be involved.

From analysis of the component calibrations, predictions that investigation of the engine without modifications would not cover an adequate range of turbine performance were verified by the engine performance. The range of turbine operation was extended by study of the engine with modifications to the compressor.

The system of analysis was also applied to prediction of the engine and component performance with assumed modifications of the burner and bearing characteristics, to prediction of component and engine operation during engine acceleration, and to estimates of the performance of the engine and the components when the exhaust gas was used to drive a power turbine.

INTRODUCTION

In order to understand better the performance characteristics of jet-propulsion engines, a research unit was designed and built at the NACA Cleveland laboratory under the direction of Eastman N. Jacobs. The operation and the interaction of the components of this unit under all possible engine operating conditions were studied. Preliminary studies of the compressor and turbine performance were first made and reported in references 1 to 4. An analysis of the component data (reference 4) showed that the constraint imposed on the turbine by operation with the compressor in the engine would limit obtainable data to a very small portion of the good efficiency range of the turbine. In fact, the range was expected to be so small that in view of the relatively large experimental errors expected in the engine data, no reliable indication of the location of the region for best turbine operation was anticipated. In order to circumvent this difficulty, two sets of engine experiments were made. After the initial investigations of the engine were completed, the compressor stator blades were reset for a lower air capacity and the engine was rerun. These two sets of data were sufficient to give a reasonably accurate picture of the turbine performance over the most important range.

From the characteristics of the components, the operation of the engine components under all possible modes of engine operation were investigated during 1946; the study included the effect of bearing and burner modifications on engine performance, operation of the engine and components during acceleration, and operation of the gas turbine and components when a power turbine is driven by the jet-engine exhaust. The basis of the analysis, which was developed for this purpose, is a simultaneous graphical solution of the equations relating compressor and turbine speed, power and gas flow, and the curves expressing the performance characteristics of compressor, bearings, burner, and turbine.

DESCRIPTION OF ENGINE

The compressor component of the engine (fig. 1) was an eight-stage compressor described in reference 1 but modified for installation in the engine by replacing the discharge

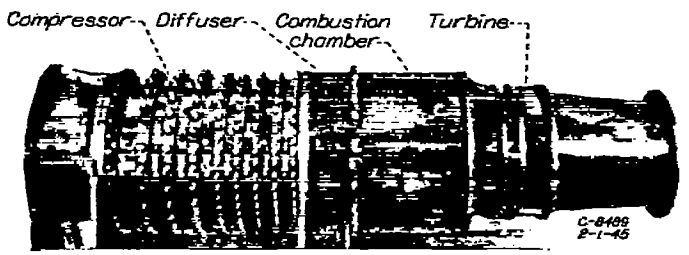

Figure 1.—NACA research jet engine.

scroll collector with an axial-flow diffuser containing a row of straightening blades. The rear-compressor journal and tapered-land thrust bearings and the turbine journal bearing were contained in a cone supported by struts from the outside wall of the diffuser (fig. 2). An outer shell bolted to the compressor casing supported the turbine casing. Inside this shell, the outer wall of the annular combustion chamber was bolted to the outlet end of the diffuser and was connected to the turbine casing with an air-tight expansion joint. The diffuser casing and the combustion chamber with part of the outer wall and the supporting shell removed is shown in figure 3; some of the 27 individual burners are

also shown. Both inner and outer walls of the combustion chamber were provided with cooling shields designed to allow air from the compressor to flow between the shields and the wall. In each burner, the fuel (propane gas) was sprayed from two bars upstream of a perforated plate, which extended across the flow area. Ignition tubes connected the combustion zones of the various burners.

The entire compressor, the diffuser, and the bearing supports were made of aluminum. Turbine rotors, rotor blades, and the first set of nozzle blades were made of Nimonic 80, second and third sets of stator blades of Vitallium, and remaining portions of the machine, which were subject to high temperatures, were made of Inconel.

The engine was designed to operate at a compressor pressure ratio of 3.36, a gas flow of 4.18 pounds per second, and a rotor speed of 13,010 rpm for a compressor-inlet temperature of 440° R and a compressor-inlet pressure of 739 pounds per square foot.

INSTALLATION AND INSTRUMENTATION

The engine inlet was connected to the laboratory refrigerated-air supply through a large stagnation chamber and the engine outlet was connected to the altitude exhaust system. The stagnation chamber, the compressor, and the turbine were completely lagged. Straighteners and screens were installed in the stagnation chamber to give uniform gas flow at the compressor inlet.

Air flow was measured in the inlet ducting of the engine with a calibrated variable orifice of ±1½-percent accuracy. Fuel flow was measured with a standard A.S.M.E. thin-plate orifice.

The location of other instrument stations is shown in figure 2. Three iron-constantan thermocouples and two static-pressure taps were located at the compressor inlet (station 1)

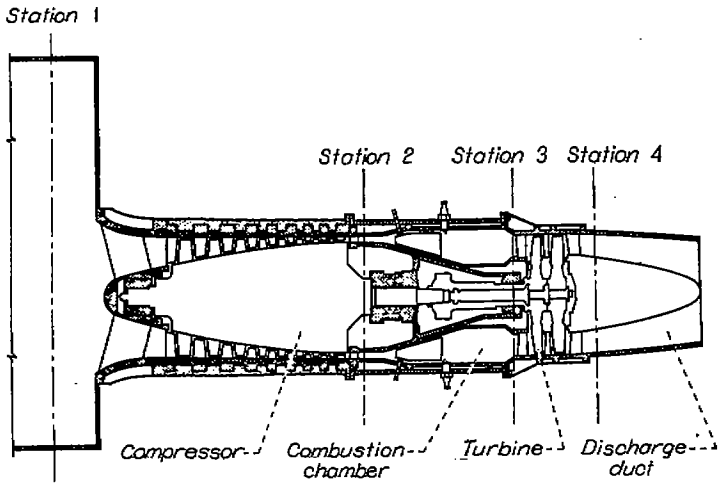

FIGURE 2.—Schematic section of engine showing measuring stations.

in the stagnation chamber. Inasmuch as the velocity in this chamber was very low, the static pressures and the observed temperatures were considered to be equivalent to the stagnation conditions. At the compressor outlet (station 2) were located three total-pressure tubes, three thermocouples, and two static-pressure taps. The iron-constantan thermocouples were equipped with recovery heads. Temperature readings were accurate to 0.5 percent of the differential from 32° F. When the data were averaged, the total-pressure readings were weighted for local mass flow.

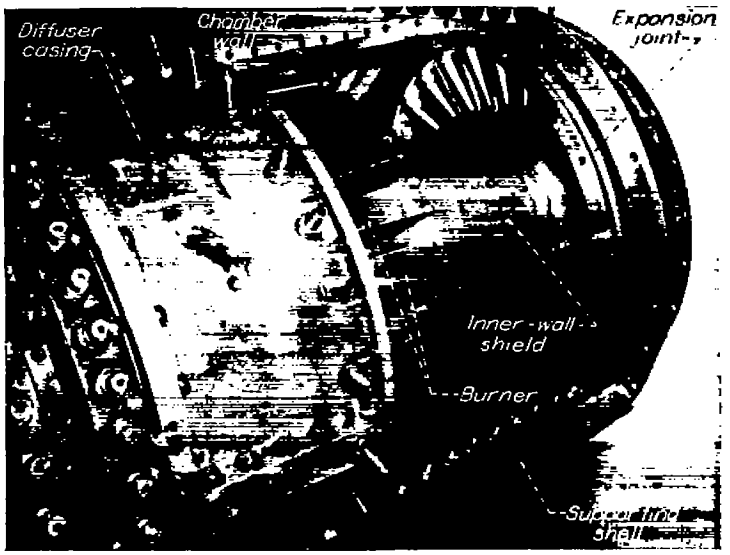

FIGURE 3.—Burners and combustion-chamber structure.

At the inlet to the turbine (station 3), six thermocouples and six total-pressure tubes were installed. The thermocouples used at the turbine inlet were shielded as shown in figure 4. This construction shielded the thermocouple and provided ventilation. Conduction of heat away from the junction was reduced by bathing a section of the thermocouple tip in flowing hot gases. Because the data obtained from these thermocouples often showed gas-temperature variations as great as 800° F at the turbine inlet, an average of the six temperature readings was not considered accurate enough for use in calculating performance. The principal use of these thermocouples was to determine the engine operating conditions. Chromel-alumel thermocouples were used at this station and the thermocouples were read within 2 percent of the differential from room temperature.

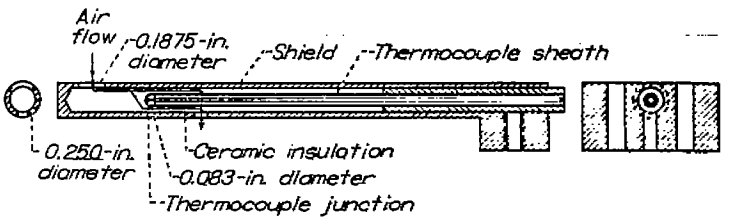

FIGURE 4.—Shielded-type thermocouple composed of chromel-alumel thermocouple wire and Inconel shield and sheath material.

At the turbine outlet (station 4), readings of total pressures and temperatures were taken downstream of the straightening vanes and between the struts supporting the streamline tail cone. At this station, no tangential velocity component was assumed to exist. Six total-pressure tubes and nine chromel-alumel thermocouples were used at this station. Although six of the thermocouples had recovery heads and three were of the shielded type used in the turbine inlet, no significant differences in readings of the two types were noted. Variations in temperature readings between

various stations indicated a probable error of the mean value of the exhaust temperature varying from about 2° to 33° F. This error caused no error in the enthalpy drop in the turbine ΔH_t, equivalent isentropic enthalpy drop in the turbine $\Delta H_{s,t}/\theta_{T,3}$, equivalent turbine torque $W_3\Delta H_t/(n\sigma_{T,3}\theta_{T,3})$, and equivalent turbine gas flow $W_3 n/(\sigma_{T,3}\theta_{T,3})$, but did result in a maximum probable error of 1 percent in equivalent turbine gas flow $W_3/(\sigma_{T,3}\sqrt{\theta_{T,3}})$ and equivalent turbine speed $n/\sqrt{\theta_{T,3}}$ and a maximum probable error of 2 percent in equivalent turbine enthalpy drop $\Delta H_t/\theta_{T,3}$ and turbine efficiency. (All symbols are defined in the appendix.)

Shaft speed was measured by an alternating-current generator built into the compressor. The rotative frequency was determined by comparison of the output frequency of the built-in alternator with that of a calibrated variable-frequency generator. These measurements were accurate to within 1 percent.

Thermocouples were also installed in the oil lines and on the bearings in order to determine the bearing power losses and oil viscosity.

PROCEDURE AND CALCULATIONS

Inaccuracy of the measured turbine-inlet temperature and the unknown heat losses made it impossible to determine from the inlet- and outlet-gas temperatures the mechanical-power input from the gas to the turbine rotor with the desired accuracy. This power was computed by adding the power output of the compressor to the gas and the power absorbed by the bearings.

The bearing-power consumptions were determined from the heat absorbed by the lubricating oil. The front compressor bearing had a separate oil supply from the remainder of the bearing system, which consisted of rear compressor and turbine bearings contained between the compressor and the turbine. In order to reduce the heat-transfer error to a minimum while the bearing power was calibrated, the inlet-air temperature was matched with the mean oil temperature while the front-bearing power consumption of the compressor was measured over a range of speeds. In calibrating the rear-bearing system, the compressor-outlet-air temperature was matched with the mean oil temperature for the system. The rear bearing was then calibrated over a range of engine air pressures in order to vary the thrust but no effect of load on the thrust bearing could be found. When the bearing-power consumptions were reduced to equivalent values for a mean oil temperature of 100° F, both sets of bearings showed a power absorption exactly proportional to the square of the speed.

The range of conditions for operation and study of the engine was limited by several factors. Simulated high-altitude operation had to be avoided because of the failure of the burners to operate satisfactorily with low pressure. There were two limitations on the temperature of the intake air: (1) Inasmuch as the compressor was made of aluminum, the inlet-air temperature was so limited that the compressor-outlet-air temperature did not exceed 300° F because of the reduction in the yield stress of this metal above 300° F; and (2) because investigation of the performance over a wide range of the ratio of turbine-inlet-gas temperature to compressor-inlet-air temperature T_3/T_1 was desirable, very cold inlet air had to be used to explore engine operation at high values of this parameter without exceeding the maximum safe metal temperature of the turbine. Periodic checks during the course of the experiments revealed that no creep of the wheel had taken place after 76 hours of engine operation at or below a gas temperature of 1250° F. The turbine rotor blades rubbed on the casing at the conclusion of a 4-hour period of operation at 1350° F with speeds varying from 110 to 215 rps. Subsequent measurements showed that the first rotor had stretched 0.067 inch and the second rotor, which was about 150° F cooler, stretched 0.005 inch. The radial stress at the blade roots was estimated to be 16,000 pounds per square inch. For this stress, static-stress data on Nimonic 80 showed that the critical metal temperature was in the region of 1200° to 1250° F. Succeeding operating gas temperatures were consequently limited to 1250° F and no further difficulties were noted.

Engine data were obtained over a variable range of the equivalent compressor speed $n/\sqrt{\theta_{T,1}}$ and the equivalent temperature ratio $\theta_{T,3}/\theta_{T,1}$

where

n rotative speed of engine, (rps)

θ ratio of square of sonic speed of gas to square of sonic speed for normal air

Subscript T denotes stagnation condition. Numerical subscripts indicate conditions at stations shown in figure 2. Because the measured turbine-inlet temperatures were not considered exact enough for computation of $\theta_{T,3}/\theta_{T,1}$, these temperatures were computed from the turbine-outlet temperatures and from the bearing and compressor power. Operating conditions of the engine were approximately set for desired values of $\theta_{T,3}/\theta_{T,1}$ from the readings of the turbine-inlet thermocouples by using

$$\frac{\theta_{T,3}}{\theta_{T,1}}=\frac{\gamma_3 R_3 T_{T,3}}{\gamma_1 R_1 T_{T,1}}\sim\frac{T_{T,3}}{T_{T,1}}$$

where

R gas constant, (ft-poundal/(lb) (°R))

γ ratio of specific heats

The ratio $T_{T,3}/T_{T,1}$ was set at values from 4.43 to values for fuel input of zero. Corrected compressor speeds varied from 90 to 290 rps.

The enthalpy rise of the air in the compressor was determined from the stagnation inlet- and outlet-air temperatures and the tables of reference 5. The isentropic enthalpy rise was computed from the stagnation pressures $p_{T,1}$ and $p_{T,2}$ and the same tables. For the turbine, the enthalpy of the exhaust gas was determined from the exhaust temperature $T_{T,4}$, the fuel-air ratio f, and the charts of reference 6. The enthalpy drop in the turbine was then determined from the equation

$$W_1(1+f)(H_{T,3}-H_{T,4})=W_1(H_{T,2}-H_{T,1})+P_a$$

where

H enthalpy, (ft-poundal/lb)

P_a power absorbed by bearings, (ft-poundal/sec)

W_1 mass flow through compressor, (lb/sec)

This computation with measured values for f and $p_{T,3}$ completely established the state of the gas at station 3. The isentropic enthalpy drop through the turbine was then computed from $H_{T,3}$, f, $p_{T,3}$, $p_{T,4}$, and the charts of reference 6.

In reference 4, the range of turbine operation obtainable from engine experiments was predicted to be insufficient for accurate determination of efficiency contours and location of region of highest efficiency. This prediction was verified by the results on the engine. The range of turbine operation was then extended by resetting the stator blades of the compressor for a lower air flow and the experiments were then repeated. Only one resetting of the compressor stator blades was necessary to cover a sufficient range of turbine operation.

PERFORMANCE OF COMPONENTS

From the engine experiments, the performance of the compressor, the combustion chamber, and the turbine components were separately evaluated. Curves faired through these data were then used to evaluate the engine performance and to examine the interaction of the engine components.

COMPRESSOR PERFORMANCE

If a small Reynolds number effect is assumed, the complete compressor performance is determined by any two independent parameters, provided all parameters are dimensionless or are given in equivalent values. If the independent variables chosen are the equivalent speed $n/\sqrt{\theta_{T,1}}$ and the equivalent air weight flow $W_1/(\sigma_{T,1}\sqrt{\theta_{T,1}})$, these variables determine the dependent parameters $\Delta H_{s,c}/\theta_{T,1}$ and $\Delta H_c/\theta_{T,1}$

where

$\Delta H_{s,c}$ isentropic rise in stagnation enthalpy, (ft-poundal/lb)

ΔH_c stagnation enthalpy rise of air in compressor, $H_{T,2}-H_{T,1}$, (ft-poundal/lb)

The compressor efficiency is the ratio of these two parameters. The pressure ratio $p_{T,2}/p_{T,1}$ is a function only of the equivalent isentropic enthalpy rise $\Delta H_{s,c}/\theta_{T,1}$ and the temperature ratio is a function only of the equivalent enthalpy rise $\Delta H_c/\theta_{T,1}$. In order to obtain good fairing of the compressor data, functions of the four fundamental parameters just described were used instead of the original parameters. These parameters were constructed to reduce the dependence of the resultant functions on compressor speed. With the parameters $\Delta H_{s,c}/n^2$ and $\Delta H_c/n^2$ as ordinate and abscissa, curves were faired through the data for constant speeds and not only the data for one particular speed but also the data for other speeds were considered. A systematic effect of inlet-air temperature was noticeable. A plot of data selected for mean compressor-air temperature equal to the room temperature showed much better correlation, which indicates the effect of heat lost to the room air. The resultant plot is shown in figure 5. The straight lines are contours of constant efficiency. The discontinuity, which may be seen in all curves, indicates the incidence of compressor surge. The portion of the curves in the region of low efficiency represents operation in a region that is normally the surge region although no fluctuation in compressor-outlet-air pressure was noticed during operation of the engine.

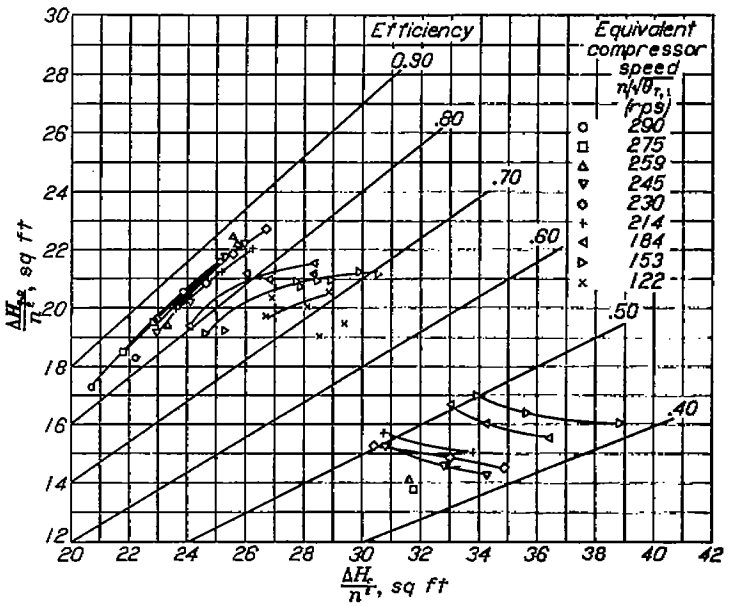

FIGURE 5.—Selected compressor data.

An additional chart is required to express the relation between the compressor air flow and the other compressor performance variables. This chart is a plot of pressure ratio $p_{T,2}/p_{T,1}$ against the air-flow parameter $W_1n/(\sigma_{T,2}\theta_{T,2})$ for constant values of the equivalent compressor speed $n/\sqrt{\theta_{T,1}}$, as shown in figure 6. Only the data used in figure 5 (mean compressor air temperature equal to room temperature) are plotted on this chart. When any uncertainty existed as to the fairing of the curves, the data for several of the speeds were plotted on a chart that showed little speed effect ($\Delta H_{s,c}/n^2$ and $W_1/(\sigma_{T,1}n)$ as coordinates with contours for constant speeds $n/\sqrt{\theta_{T,1}}$). Thus, the data allowed several speeds to be considered in fairing a curve for any one speed. The region beyond the surge line for each curve in figure 6 is shown connected with the normal operating portion by a dashed line indicating the absence of any data for that section of the curve.

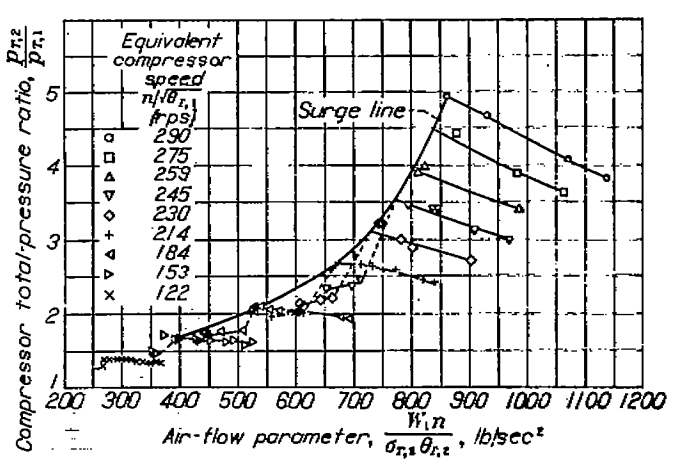

FIGURE 6.—Selected compressor-pressure-ratio and air-flow data.

TURBINE PERFORMANCE

For correlation of the turbine performance, the corrected turbine gas flow was plotted with the equivalent isentropic enthalpy drop. No effect of speed was observed; a definite grouping of the data, however, took place according to the turbine-inlet temperature. This grouping is shown in figure 7 where the data for turbine-inlet temperatures of 190°, 500°, and 1250° F are plotted. The curve for an inlet temperature of 190° F, shown for comparison, was obtained from the data of reference 4, which reports the turbine performance obtained from calibrating the turbine component alone by the use of air at 190° F. The gas flow at 1250° F is from 6 to 17 percent higher than the gas flow for the same pressure ratio at 190° F and was believed to be caused by variation in the leakage flow through the blade-tip clearance space, which changed with gas temperature. In order to account for this discrepancy, a very crude method was used to estimate the leakage. According to reference 7, the leakage flow may be estimated by assuming twice the mass flow per unit area in the clearance space as for the rest of the annular area of the turbine. If a linear variation of the temperature of the wheel and the blades varying from 200° F at the center of the wheel to the turbine-inlet stagnation gas temperature at the tips of the blades and a casing temperature equal to turbine-inlet stagnation gas temperature are assumed, the clearance flow space could be computed for each temperature. The wheel runs cooler than the insulated case and as a result of the metal expansion, the clearance will expand with increasing temperature. When the gas-flow data were corrected for clearance variations from measured values of W_3 to values of W_3', which correspond to operation at a turbine-inlet temperature of 190° F, the data showed no variation of gas flow for temperature, rotative speed of the turbine, or indicated whether the data were obtained from engine- or turbine-component experiments (fig. 8). All turbine-performance parameters for which the symbols are primed have thus been corrected for the effect of leakage. The enthalpy drop is corrected by assuming that no work was obtained from the leakage air.

In order to obtain complete correlation of the turbine performance, an additional chart presenting corrected work output at constant values of equivalent speed is required.

Because of the inability to measure accurately the turbine-inlet temperature, the turbine equivalent speed could not be accurately set at preassigned values during engine operation and turbine data could not be directly plotted for constant equivalent speeds. An auxiliary chart was therefore prepared by plotting curves of $W_3'\Delta H_{s,t}/(n\sigma_{T,3}\theta_{T,3})$ against $W_3'n/(\sigma_{T,3}\theta_{T,3})$ for constant assumed values of $n/\sqrt{\theta_{T,3}}$. These curves were directly obtained from the faired curve of figure 8 (b), which showed no speed effect and which was considered to have perfect correlation. The efficiency contours as indicated by the data were then drawn and the corrected work output was determined from the isentropic work and efficiency values. A typical curve of corrected equivalent enthalpy drop against the equivalent isentropic enthalpy drop for an equivalent speed of 135 rps is shown by the solid curve in figure 9. Also shown are data obtained for equivalent turbine speeds between 130 and 140 rps. There are two sets of engine data shown: one set from the engine with the original settings of the compressor blades that correspond to the performance curves in figures 5 and 6; and the second blade settings, which were merely used to explore a larger operational range of the turbine. The importance of this procedure may be seen from figure 9, which shows that the data obtainable with the original blade settings are insufficient to give reliable efficiency curves because of the short range and the experimental errors.

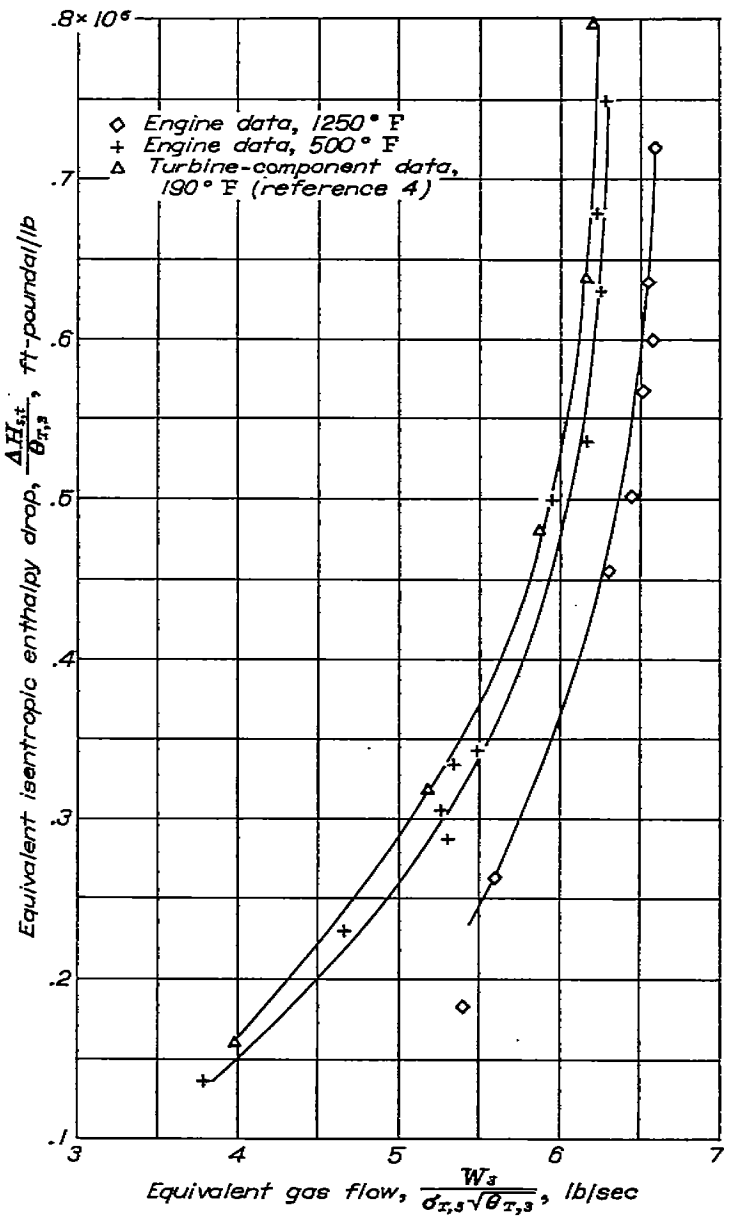

FIGURE 7.—Equivalent isentropic enthalpy drop and gas flow through turbine with various gas temperatures.

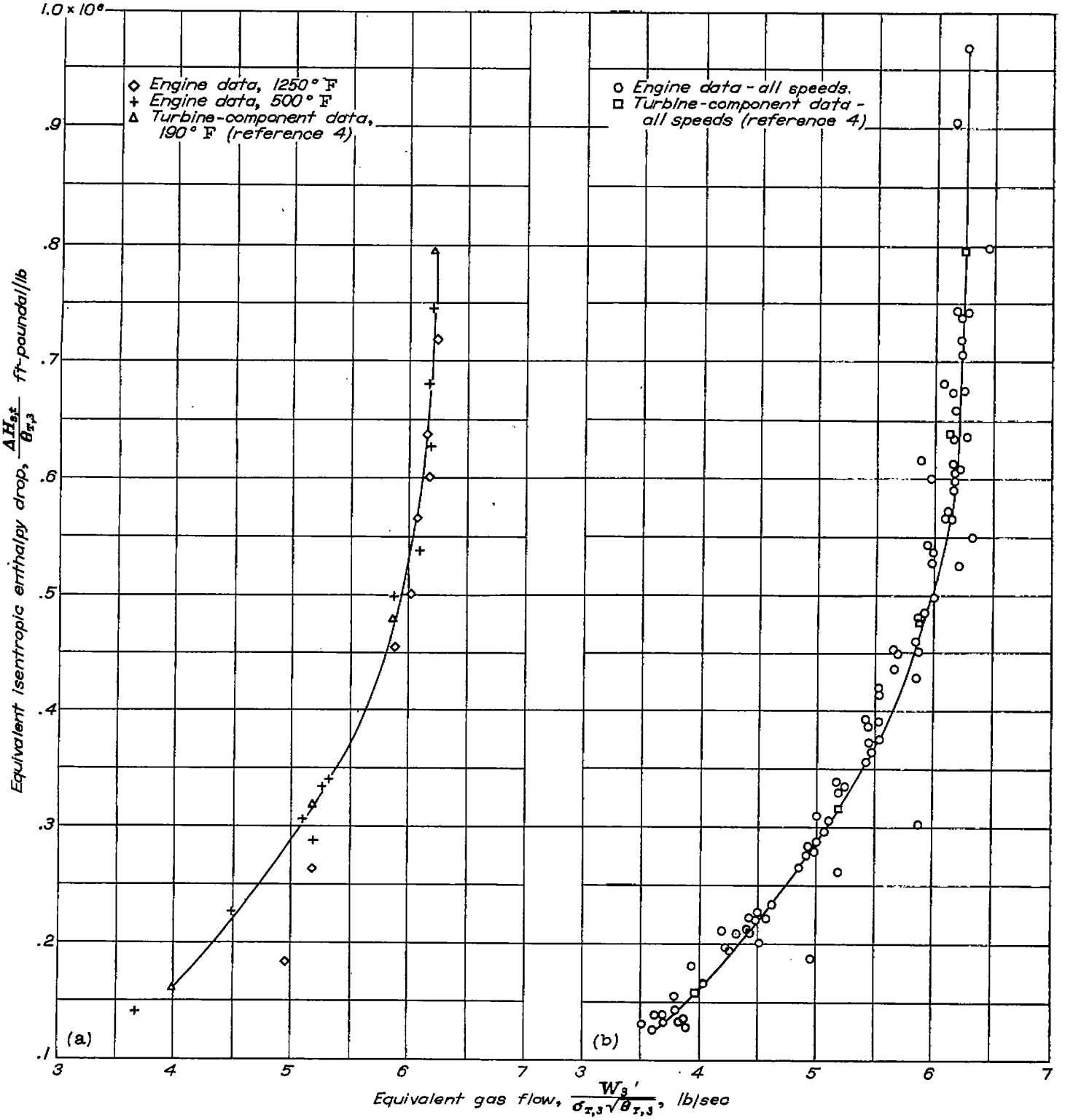

(a) Corrections applied to data of figure 7.

(b) Data for all temperatures and speeds.

FIGURE 8.—Equivalent isentropic enthalpy drop and gas flow through turbine corrected for clearance expansion.

Also shown on the charts for comparison are the results obtained from the turbine-component experiments (reference 4). The discrepancies shown are unaccounted for. In some cases agreement is good, but where there is disagreement the data obtained in the engine experiments show a more rapid variation of efficiency with variation in enthalpy drop. The complete plot of turbine performance is shown in figure 10. A speed for maximum efficiency is 155 rps, which is closer to the design value of 136 rps than was the indicated optimum speed (180 rps) measured with cold air (reference 4). One possible reason for the shift in speed at maximum efficiency is the heat loss from the gas at high

temperatures of operation. With heat loss through the wheel as well as to the casing, the volumetric expansion of the gas after passing through the first turbine stage would be less than when the engine was run with cold air. Consequently, the second-stage gas velocities would be decreased and lower wheel speeds would be required for optimum operation of the second stage. This explanation does not account for the local efficiency maximum in the region of an equivalent speed of 85 rps.

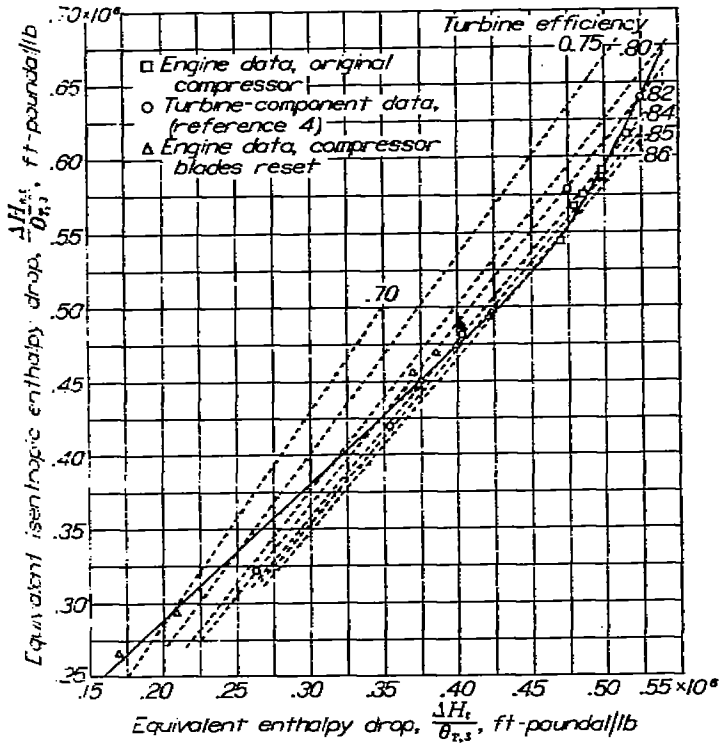

FIGURE 9.—Ideal and actual work output of turbine at equivalent turbine speeds between 130 and 140 rps. Solid curve faired for 135 rps.

Because of this effect of heat transfer on efficiency, characteristics obtained with hot gas are desirable if turbine-component experiments are considered necessary.

This shift in efficiency will probably be very much smaller for a single-stage turbine than for a multistage turbine because the volumetric change caused by heat loss primarily affects operation of second or later stages.

It will be obvious from subsequent analysis that with a turbine, which operates choked or nearly so in the first stage, accurate estimates may be made of compressor operation in the engine from component data even if the turbine efficiencies are in error, provided that accurate mass-flow characteristics of the turbine are available.

COMBUSTION CHAMBER

The other significant component of the engine is the combustion chamber. Two variables depending on combustion-chamber performance are needed to determine the over-all engine performance, the pressure ratio $p_{T,3}/p_{T,2}$, and the combustion-chamber efficiency η.

Pressure loss.—The combustion-chamber pressure loss consists of two components: (1) the friction loss, which is independent of the burning process, and (2) the momentum

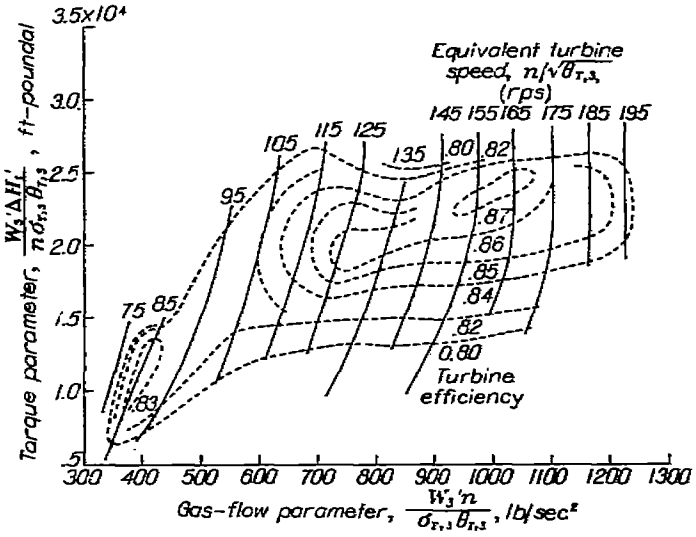

FIGURE 10.—Corrected performance of turbine in parameters for engine computations.

pressure loss, which depends on the over-all temperature ratio $T_{T,3}/T_{T,2}$ of the combustion chamber. An analysis of these losses based on an idealized form of the combustion chamber is made in reference 8. The data obtained could not be correlated on the basis of this analysis. Aside from possible inaccuracies of the data, another probable cause of the discrepancy is indicated by the fact that some of the data showed lower pressure loss with increased combustion rates for comparable air flows. This anomaly is impossible with the assumption of a tubular combustion chamber of uniform flow area, as is indicated in reference 8. In this engine, the combustion-chamber flow area expanded and the flow diffused between the compressor and the combustion zone and, to some extent, in the combustion zone. The introduction of a resistance, such as a screen at the outlet of a diffuser, increases the efficiency of the diffuser (reference 9). Combustion in the chamber of the engine acts as a resistance to the flow in a manner similar to a screen with a greater pressure drop in the combustion region of the higher local velocities. With such an effect, the data could not be satisfactorily correlated on a simple basis, and for the analysis, the assumption was made that the empirical relation

$$p_{T,2}-p_{T,3}=0.4665\,\frac{W_1'^2}{\rho_{T,2}}\ \text{(lb/sq ft)}$$

could be used, where ρ is the gas density in pounds per cubic foot. This constant was obtained from the data and yielded values that show extreme variations of 2.5 percent in absolute pressure at the turbine inlet. For the highest gas flow, the mean deviation of the absolute pressure is only 0.8 percent.

Combustion efficiency.—Combustion efficiency was computed from the equation

$$\eta=\frac{(H_{T,3}-H_{T,2})+f(H_{T,3}-H_f)}{fh}$$

where

f fuel-air ratio
h heating value of fuel, (ft-poundal/lb)
H_f enthalpy of incoming fuel, (ft-poundal/lb)

This definition of η is equivalent to the ratio of the effective heating value of the fuel in increasing the enthalpy of the mixture to the actual heating value. According to an unpublished analysis conducted at the NACA Cleveland laboratory, it should be possible to obtain a correlation of the combustion efficiency with other combustion-chamber variables by a relation of the form

$$\log\,(\eta\sqrt{T_{T,3}})=a-b/T_{T,3}$$

where the quantities a and b are only functions of the variable $W/\sqrt{p_{T,2}}$. Such a correlation was attempted with the data available by grouping data of nearly equal values of $W\sqrt{p_{st}/p_{T,2}}$ where p_{st} is standard atmospheric pressure. This plot shows excellent correlation of the data from $T_{T,3}$ of 640° F to the maximum temperature of engine operation (fig. 11). A critical value of the parameter $W\sqrt{p_{st}/p_{T,2}}$ exists at approximately 3.6 pounds per second, below which there is a sharp drop in combustion efficiency. Because $W\sqrt{p_{st}/p_{T,2}}$ decreases with increasing altitude, a critical altitude of the engine will occur above which the combustion efficiency of the burner will drop off quite rapidly. During operation of an engine with a burner having such characteristics, no change in the internal aerodynamics of the engine would be noted; the engine would merely require more fuel to operate at the desired speed and temperature.

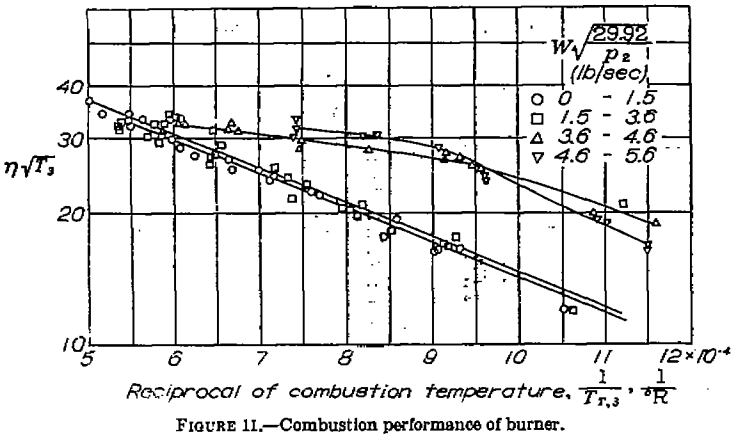

FIGURE 11.—Combustion performance of burner.

INTERACTION OF ENGINE COMPONENTS

STEADY-STATE JET-ENGINE OPERATION

For determination of the operation of the compressor-turbine combination in a jet engine, the relations between the compressor and turbine parameters must be used. When no external leakage is assumed, the weight flow through the compressor plus the fuel added is equal to the weight flow through the turbine. Therefore

$$W_1=\frac{1}{(1+f)}\,W_3$$

Because the use of weight flow through the turbine corrected for clearance expansion is desirable, a clearance correction $F_z(T_{T,3})$, which is a function of the turbine temperature, is employed so that W_3' is the weight flow corrected for clearance flow and $W_3=F_z(T_{T,3})W_3'$ is the actual weight flow through the turbine. The resultant equation in terms of corrected parameters is

$$\frac{W_1 n}{\sigma_{T,2}\theta_{T,2}}=\left[\frac{1}{(1+f)}\,\frac{\gamma_3 p_{T,3}}{\gamma_2 p_{T,2}}\,F_z(T_{T,3})\right]\frac{W_3' n}{\sigma_{T,3}\theta_{T,3}} \qquad (1)$$

This equation is more complete than the corresponding one given in reference 4 because of the inclusion of the temperature correction for leakage variation. The compressor-outlet conditions are used to correlate compressor air flow because the compressor-outlet pressure is nearly equal to that at the turbine inlet. The usual equivalent air-flow parameter is multiplied by the equivalent speed to obtain the product $\sigma_{T,2}\theta_{T,2}=\frac{\gamma_2 p_{T,2}}{\gamma_0 p_0}$ in the gas-state correction factor, thus eliminating the temperature, which would cause a large difference between the compressor and turbine air-flow parameters. These air-flow parameters for the compressor and the turbine are simple combinations of the usual equivalent variables, which are used to correlate compressor and turbine data with only small variations of performance in terms of this parameter over a wide range of gas pressures and temperatures. In the engine, the use of variables such as this variable largely eliminates the effects of altitude, ram, or nozzle setting on compressor or turbine performance in terms of equivalent variables. Factors that were neglected are the effect of changes in Reynolds number and heat loss on engine performance. In equation (1), the correction term in brackets is near unity.

The turbine-power output is absorbed by compressor, bearings, and other accessories. Because enthalpy change is the energy input per pound of gas,

$$W_1\Delta H_c+P_a=W_3\Delta H_t$$

where P_a is the power absorbed by the bearings and the accessories. In terms of corrected equivalent parameters,

$$\frac{W_1\,\Delta H_c}{n\sigma_{T,2}\theta_{T,2}}+\left[\left(\frac{P_a}{n\sigma_{T,1}\theta_{T,1}}\right)\left(\frac{\gamma_1 p_{T,1}}{\gamma_2 p_{T,2}}\right)\right]=\left[F_m(T_{T,3})\frac{\gamma_3 p_{T,3}}{\gamma_2 p_{T,2}}\right]\left(\frac{W_3'\Delta H_t'}{n\sigma_{T,3}\theta_{T,3}}\right) \qquad (2)$$

The torque was used rather than the power in order to avoid directly involving the temperature. The correction terms in brackets introduce a small discrepancy between the compressor and turbine parameters, which have the dimension of torque. The function $F_m(T_{T,3})$ is a correction term for torque as affected by clearance expansion at various turbine temperatures. Thus if the prime indicates the value corrected to some standard clearance, the actual turbine-torque parameter is

$$\frac{W_3\,\Delta H_t}{n\sigma_{T,3}\theta_{T,3}}=F_m(T_{T,3})\left(\frac{W_3'\Delta H_t'}{n\sigma_{T,3}\theta_{T,3}}\right) \qquad (3)$$

In order to evaluate the correction terms, the operating conditions of the engine must be known. Because the effect of these terms is slight, the engine operating conditions need be known only approximately. The engine operation may first be estimated, assuming no corrections, and then the correction terms evaluated. The process may be repeated if desired after the engine operating conditions have been determined with greater accuracy.

Because the torque parameter $\frac{W_1 \Delta H_c}{n\sigma_{T,2}\theta_{T,2}}$ is nearly equal to $\frac{W_3'\Delta H_t'}{n\sigma_{T,3}\theta_{T,3}}$ and the air-flow parameter $\frac{W_1 n}{\sigma_{T,2}\theta_{T,2}}$ is nearly equal to $\frac{W_3' n}{\sigma_{T,3}\theta_{T,3}}$, the compressor and turbine characteristics are plotted in terms of these variables with constant-speed contours. The compressor chart is shown in figure 12. The portions of the curves detached from and to the left of the nearly straight sections represent the region of low air flow and low efficiency, normally in a region of lower air flow than the surge line. A plot of the same variables for the turbine with efficiency contours included is shown in figure 10.

The approximate simultaneous operation of both the compressor and the turbine is obtained by superimposing the compressor and turbine charts (figs. 10 and 12). Any one point on the compounded chart represents an operating state for both the compressor and the turbine when they are coupled together in the engine. This point has associated with it an equivalent compressor speed $n/\sqrt{\theta_{T,1}}$ and an equivalent turbine speed $n/\sqrt{\theta_{T,3}}$. Because the compressor and turbine speeds are equal, the ratio of the equivalent speeds is the square root of the corrected temperature ratio:

$$\frac{n/\sqrt{\theta_{T,1}}}{n/\sqrt{\theta_{T,3}}}\sqrt{\frac{\theta_{T,3}}{\theta_{T,1}}} \tag{4}$$

It is thus possible to establish lines of constant equivalent temperature ratio on the compound chart. Any compressor- and turbine-performance variable may then be determined as a function of the compressor equivalent speed and the engine equivalent temperature ratio.

In order to correct this estimate of engine performance for changes in gas properties, bearing power, leakage losses, and combustion-chamber pressure losses, the altitude of operation is assumed, and the correction terms in equations (1) and (2) are evaluated by means of the approximate correction factors obtained and by making use of the burner characteristics and other auxiliary curves. These corrections applied to the compressor curves give approximate turbine operating conditions required to drive the engine and the resulting curves may be superimposed on the turbine performance charts as were the original uncorrected com-

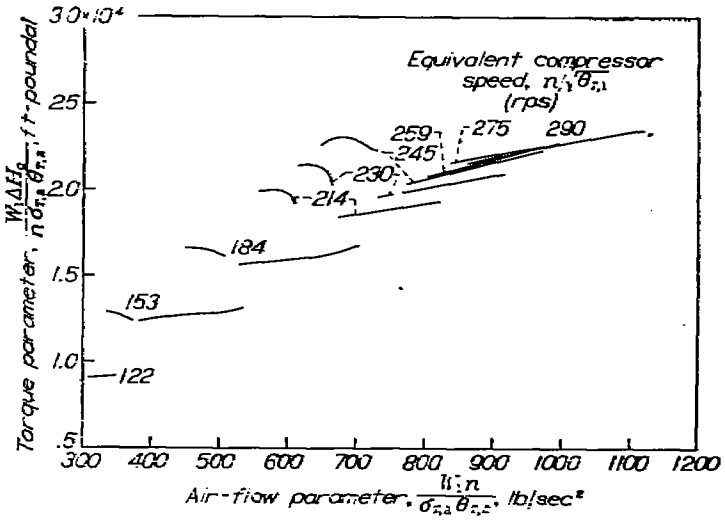

FIGURE 12.—Compressor performance in parameters for engine computations.

pressor curves. The process may be repeated if desired for additional accuracy. A set of compressor curves with the corrections introduced and then superimposed on the turbine characteristics is shown in figure 13. The corrections used are based on an inlet-air temperature $T_{T,1}$ of 480° R and an inlet-air pressure $P_{T,1}$ of 1414 pounds per square foot. The heavy line is the surge line. The high-speed range of the compressor is in the region of decreasing turbine efficiency and close to optimum efficiency. A reduction in bearing torque would lower these curves to the center of the high-efficiency region.

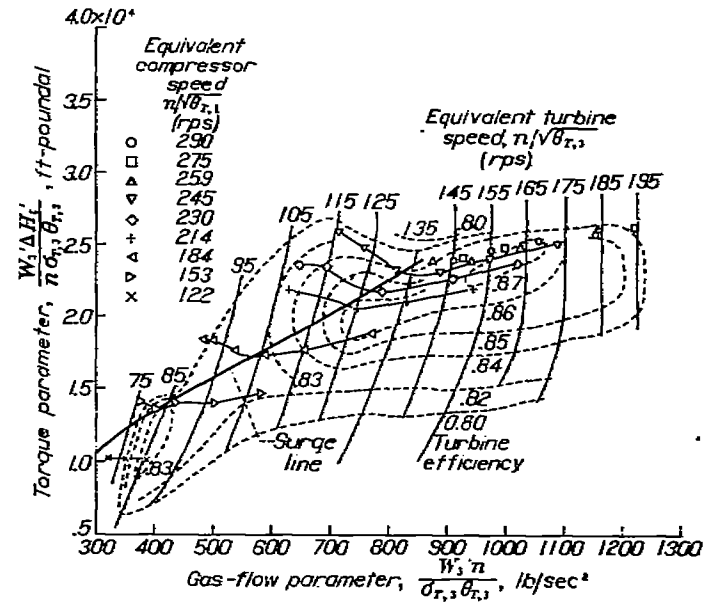

FIGURE 13.—Matching chart based on engine experiments. Component performance corrected for losses, clearance expansion, and change in gas properties. Compressor-inlet stagnation temperature and pressure, 480° R and 1414 pounds per square foot, respectively.

If the turbine air flow is accurately known as a function of the pressure ratio (or equivalent isentropic enthalpy drop), it is clear that on this figure the turbine curves will shift vertically. Because of the large slope of these curves, the intersections with the compressor curves will be very little affected by such an efficiency error and no effect would be observed for choking of the turbine, inasmuch as this condition results in vertical turbine curves. Turbine pressure ratio and therefore exhaust pressure ratio would be affected by such an error. Experimental results of the turbine performance obtained with the cold-air investigation of the turbine component show excellent correlation of air-flow characteristics and slight variations of efficiency. Hence, the results of cold-air turbine-component experiments may be used to predict accurately compressor operation in the engine but slight errors in jet-power estimates would result from the use of such data.

The lines of constant corrected engine temperature ratio obtained from equation (4) are shown in figure 14. At low speeds, the highest temperature ratio that may be used without surging the compressor is 3.0. The ratio of 4.0 has only one useable compressor speed of those plotted, whereas the ratio of 4.5 is entirely in the surge region for all compressor speeds.

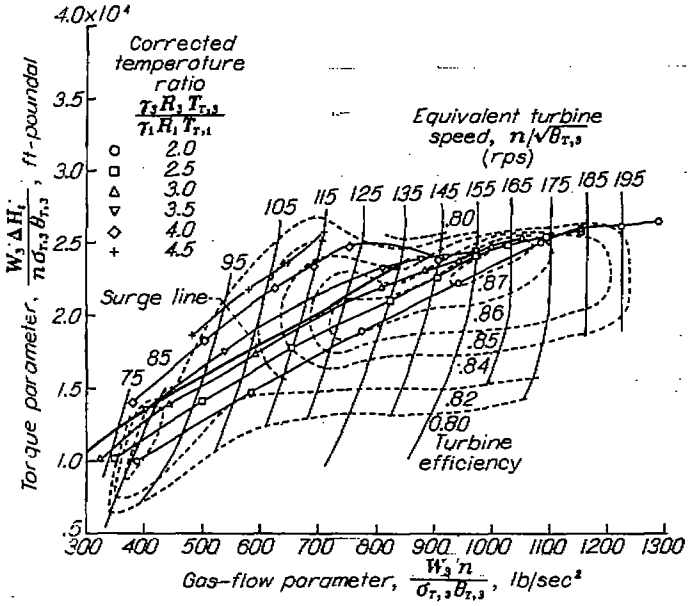

FIGURE 14.—Turbine operating conditions at various temperature ratios in engine. Compressor-inlet stagnation temperature and pressure, 480° R and 1414 pounds per square foot, respectively.

Operation of the compressor under these various conditions is shown more clearly in figure 15 where the pressure ratio is plotted against the air-flow parameter $W_1 n/(\sigma_{T,2}\theta_{T,2})$ used in matching the compressor and turbine characteristics. Lines of constant compressor speed and compressor efficiency are also shown. Engine operating conditions beyond surge are not shown although the engine was operated in this condition as shown by the extension of several of the compressor speed lines beyond the region of peak pressure ratio. Surge limitation for temperature ratios of 3.5 and 4.0 are clearly shown.

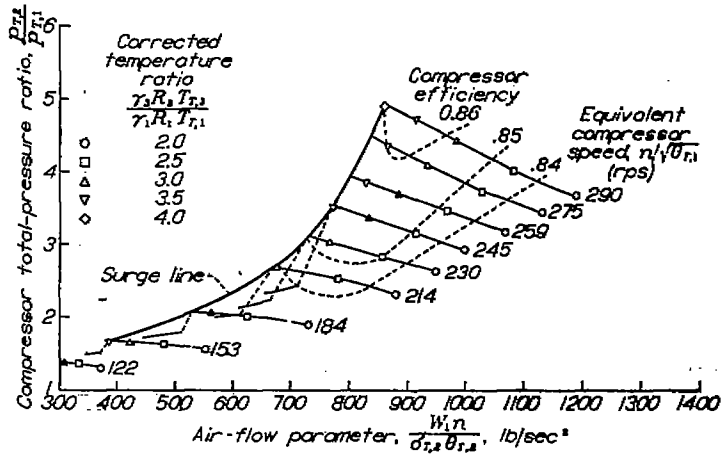

FIGURE 15.—Compressor operating conditions at various temperature ratios in engine. Compressor-inlet stagnation temperature and pressure, 480° R and 1414 pounds per square foot, respectively.

The operation of the engine at air flows lower than for peak compressor pressure ratio in what is normally the surge region was not accompanied by the usual pressure fluctuations. In varying the operation of the engine from this surge region to the normal operating range, the gas-flow parameter used in the matching chart changes by the usual small increments. This parameter, however, uses the combustion-chamber pressure to correct the weight flow. The discontinuous jump in pressure ratio therefore corresponds to a jump in the weight flow correlated on the basis of the inlet pressure. For fixed engine-inlet conditions, the actual (uncorrected) air flow through the engine will also change discontinuously. This phenomenon is illustrated in figure 16, which shows actual data for compressor speeds of 214 and 245 rps. The discontinuous increase in air flow at 214 rps is 40 percent whereas at 245 rps the increase is 50 percent. In both cases the combustion-chamber volume flow changed very little. This jump will be reflected in engine thrust when passing through the surge region.

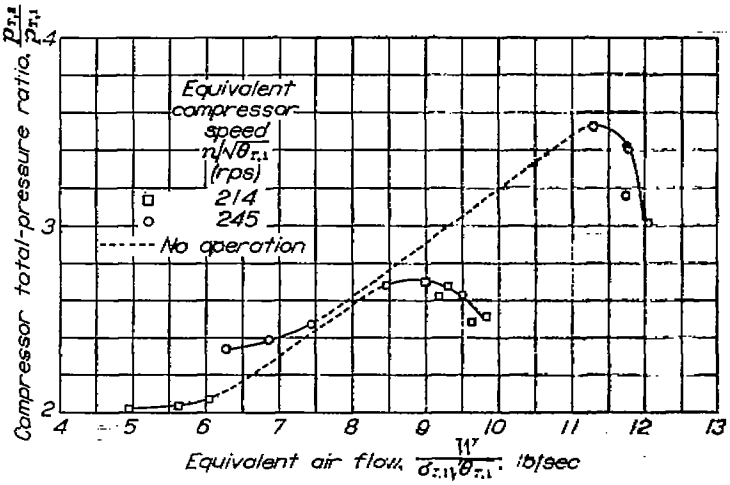

FIGURE 16.—Variation of compressor pressure ratio with inlet flow.

From this technique for computing engine operation, where the turbine characteristic curves are vertical, indicating turbine choking, the compressor performance in the engine may be accurately predicted independent of errors in the turbine efficiency. The exhaust-pressure ratio is, however, dependent on the turbine efficiency.

Over-all corrected static thrust and specific thrust of the engine were computed from the matching-chart data, with the assumption that there were no losses in the intake or the jet nozzle. The resultant performance curves, including operation at all possible ram pressures and jet-nozzle sizes, are shown in figure 17, which also shows contours of constant compressor speed and constant temperature ratio and the compressor surge line. For operation at a fixed speed, increase of the temperature ratios beyond the limit shown by the surge line causes a sharp drop in thrust and specific thrust. At a temperature ratio of 3, a thrust of 678 pounds can be obtained for a specific thrust of 1.06 pounds thrust per pound fuel per hour and a compressor speed of 290 rps. The maximum operating temperature ratio that can be used at 290 rps without surge is 4, at which condition the engine thrust is 965 pounds and the specific thrust 0.84 pound thrust per pound fuel per hour. The compressor efficiency did not begin to fall off at 290 rps so that engine thrust and specific thrust could probably be improved by operating at speeds higher than 290 rps in the high-temperature and high-thrust range.

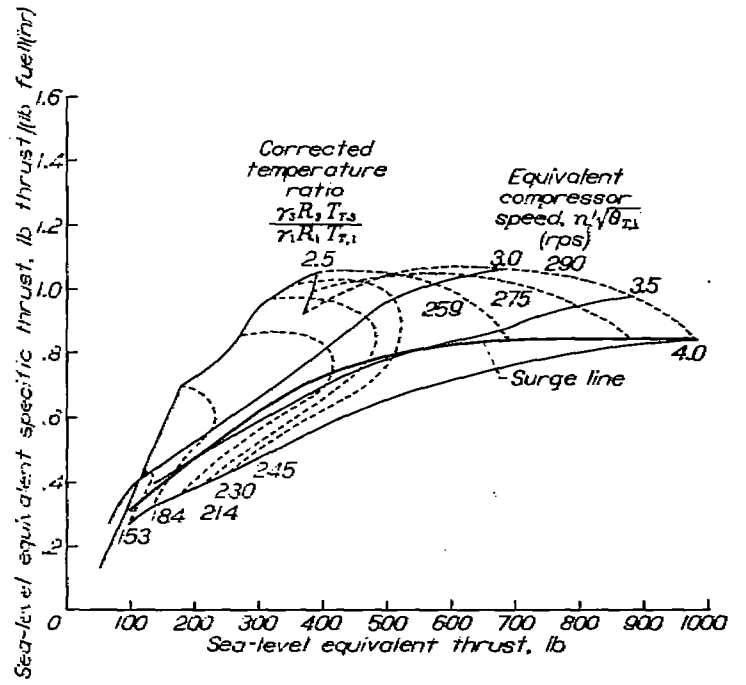

FIGURE 17.—Equivalent static performance of turbojet engine. Compressor-inlet stagnation temperature and pressure, 480° R and 1414 pounds per square foot, respectively.

ESTIMATED EFFECT OF ENGINE MODIFICATIONS

The engine data were next applied to the prediction of engine performance with assumed improvements in the components. The burner used in the engine had a peak combustion efficiency of 87 percent. Burners now available show a peak combustion efficiency of 95 percent and a friction coefficient about 40 percent of that of the burner employed in this engine. A burner with these characteristics was assumed to be installed in the engine. Another modification was the assumed installation of a set of low-friction bearings instead of the journal bearings used in the experiments. The turbine matching chart for operation at various engine temperature ratios computed on this basis for an inlet temperature of 480° R and an inlet pressure of 1414 pounds per square foot is shown in figure 18. The essential change is

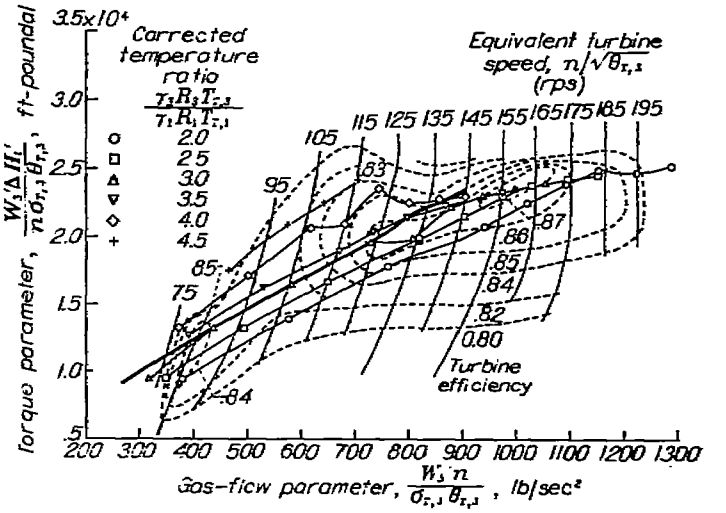

FIGURE 18.—Estimated turbine performance at various temperature ratios in engine with assumed modifications. Compressor-inlet stagnation temperature and pressure, 480° R and 1414 pounds per square foot, respectively.

the reduction in turbine torque required to operate the engine at various speeds. Operating conditions for desirable high speeds are now lowered into the region of peak turbine efficiency. The improvement of the bearings is therefore of special significance in this case because it not only allows more power for the jet but also causes the turbine to operate with higher efficiency. The point at the temperature ratio of 3.5 and a turbine speed $n/\sqrt{\theta_{T,3}}$ of 155 rps corresponding to a compressor speed $n/\sqrt{\theta_{T,1}}$ of 290 rps is in the region of peak turbine efficiency. The compressor operating conditions are only slightly changed, as shown in figure 19. The

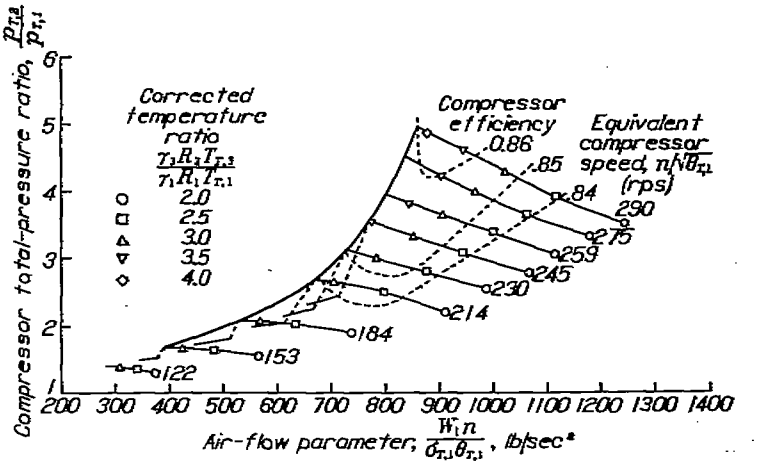

FIGURE 19.—Compressor performance at various temperature ratios in turbojet engine with assumed modifications. Compressor-inlet stagnation temperature and pressure, 480° R and 1414 pounds per square foot, respectively.

point for a temperature ratio of 3.5 and compressor speed of 290 rps is also in the region of peak compressor efficiency. The confluence of the peak compressor- and turbine-efficiency regions shows that these components are perfectly matched. The resultant performance of the modified engine is shown in figure 20. The peak specific thrust in this case is 1.24 pounds thrust per pound fuel per hour. A comparison of figures 20 and 17 shows that for a speed of 290 rps and a temperature ratio of 3.0, the thrust has been increased about 5 percent from 678 to 715 pounds, whereas the specific thrust has been increased 15 percent from 1.06 to 1.22 pounds thrust per pound fuel per hour. At a temperature ratio of 4.0 and a compressor speed $n/\sqrt{\theta_{T,1}}$ of 290 rps, the thrust has been increased 9 percent from 965 to 1050 pounds, whereas the specific thrust has been increased 21 percent from 0.84 to 1.02 pounds thrust per pound fuel per hour.

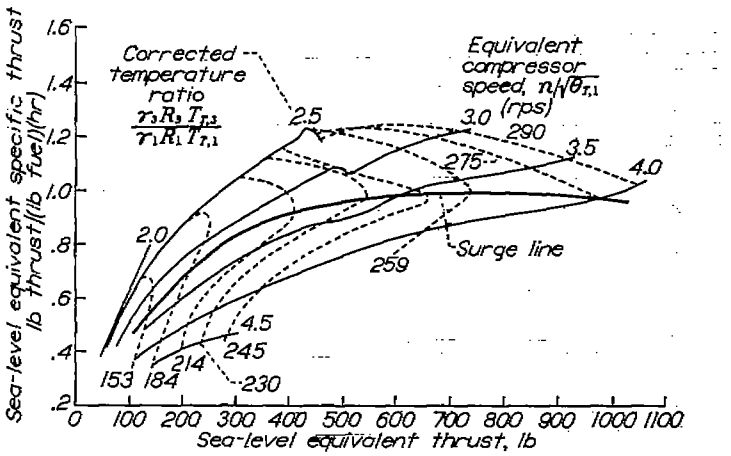

FIGURE 20.—Static performance of turbojet engine with assumed modifications. Compressor-inlet stagnation temperature and pressure, 480° R and 1414 pounds per square foot, respectively.

The point at which both the compressor and the turbine are operated at their best efficiency (at a temperature ratio of 3.5 and an equivalent speed of 290 rps) is not the region of best engine efficiency because of decreasing jet efficiency with increasing jet velocities. There will, however, be a flight speed at which the best engine efficiency simultaneously occurs with this optimum matching condition.

The engine performance estimates for both the unmodified engine and the engine with modifications are somewhat optimistic because the effect of inlet-diffuser and jet-nozzle losses were not taken into account. A reduction of about 4 to 5 percent in thrust and specific thrust would be the right order of magnitude of the correction. Also omitted from the estimate was the power consumption of the oil and fuel pumps that would normally be added to the bearing power consumption when computing engine performance. Although the absolute magnitudes of the performance parameters computed are somewhat optimistic, the effect of engine changes on the improvement of performance is conservative. In the case of the analysis that takes into account the power required for accessories, the reduction in torque would take place at a higher torque level where the turbine efficiency varied more rapidly than near the region of maximum turbine efficiency.

Under some conditions, improvement in components might not be reflected in the improvement of over-all engine performance. For example, if an engine with poor bearings is operating at a torque lower than the torque for maximum turbine efficiency, the reduction of torque requirements by improving the bearings would lower the turbine efficiency. Under such circumstances, the over-all performance of the engine might show no change resulting from improvement of the bearings.

ACCELERATION OF TURBOJET ENGINE

In order to observe the interaction of the engine components during acceleration, an estimate of the engine moment of inertia and the torque required for acceleration at the rate of 6.50 rps per second was made. This torque of 38.1 pound-feet was incorporated into the bearing-power correction term $P_a/n\sigma_{T,1}\theta_{T,1}$ of equation (2). From the form of this equation, the effect of this torque on engine operation is seen to increase inversely with the altitude pressure; acceleration is therefore more difficult at altitude conditions than at sea level. A condition of sea-level pressure was assumed for the computation. The operation of the compressor is shown for the condition of acceleration in figure 21, which shows a slight displacement from the compressor-surge region when compared with the operating condition with no acceleration. For a fixed operating temperature, the acceleration state is equivalent to opening the propulsion nozzle or reducing the back pressure on the turbine in order to obtain the increased turbine power required for acceleration. Hence, if the turbine flow is not choked, the air flow will increase and the back pressure on the compressor will be so lowered that the compressor operating-condition ratio for engine acceleration will be displaced from surge toward the region of lower temperature ratio when compared with

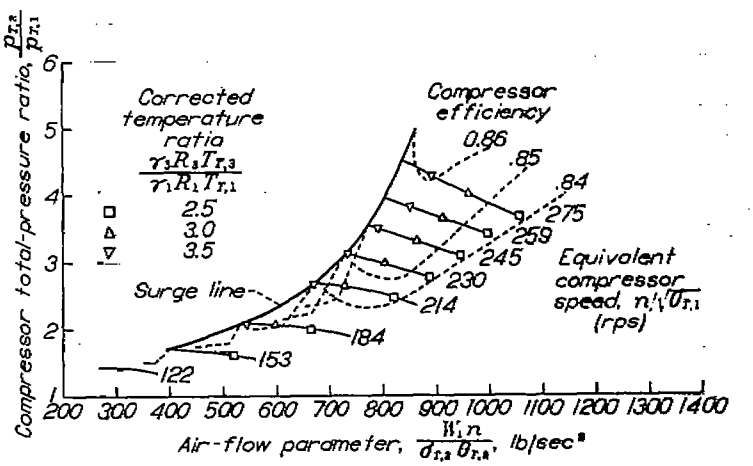

FIGURE 21.—Compressor operation with acceleration torque of 38.1 pound-feet at sea-level conditions.

the steady-state operating condition. For a choked turbine, the compressor operating condition will be the same for acceleration and for steady state with the same compressor speed and engine temperature ratio. In this case, the determination of whether the compressor will operate in the low-efficiency region beyond the surge line when increasing the fuel input for acceleration is a simple matter of examination of the new temperature-ratio point at the compressor speed for the start of acceleration. Less exhaust-nozzle pressure will be available than in the steady-state case for a given speed and acceleration temperature ratio. This fact is shown in figure 22 in which the over-all engine total-pressure ratio for various engine speeds and temperature ratios are shown under the conditions that a torque of 38.1 pound-feet is accelerating the engine. The turbine pressure ratio will increase because of the higher turbine power required for acceleration.

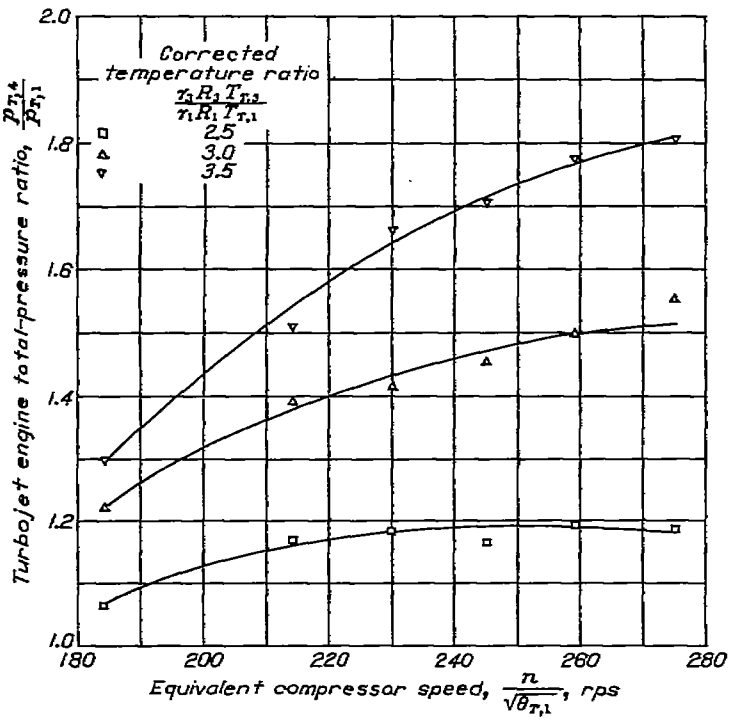

FIGURE 22.—Over-all pressure ratio of turbojet engine with acceleration torque of 38.1 pound-feet at sea-level conditions.

OPERATION AS HOT-GAS GENERATOR FOR POWER TURBINE

The compressor-turbine combination may be regarded as a machine for generating hot gas at a higher pressure than initially available. In the case of the jet engine, this gas is used to propel the airplane by this reaction. Another possible application is the use of this gas for driving a power turbine, which operates independently of the rest of the engine. The operation of such an engine was analyzed by assuming that the exhaust of the turbojet engine was used to drive a power turbine, which expanded the gas to a stagnation pressure equal to that at the compressor inlet. The pressure ratio of the gas generator was first plotted as a function of the mass flow corrected for the gas state at the turbine outlet. The pressure ratio was converted to equivalent isentropic enthalpy drop corrected for gas state at the gas-generator outlet. Contours of constant corrected compressor speed and constant temperature ratio are shown in figure 23. On the basis of such coordinates, turbine performance is independent of speed, as shown in figure 8. A turbine characteristic was computed on this assumption with a critical air flow and pressure ratio, which corresponds in figure 23 to an engine temperature ratio of 4.0 and an equivalent compressor speed of 290 rps. The flow through the first nozzle ring was assumed to be critical at a lower pressure ratio than any other set of blades of the power turbine, with the resultant isentropic enthalpy drop and flow characteristic as shown in figure 23. This curve is merely hypothetical and serves in the absence of a specific power turbine with known characteristics. Normally, each power turbine-speed characteristic would be worked separately and the efficiency would be known at each point of the curve. The intersection of this curve with the gas-generator characteristics gives for each compressor speed a fixed temperature ratio $\theta_{T,3}/\theta_{T,1}$, gas flow $W/(\sigma_{T,1}\sqrt{\theta_{T,1}})$, and power output on the assumption of a power turbine efficiency

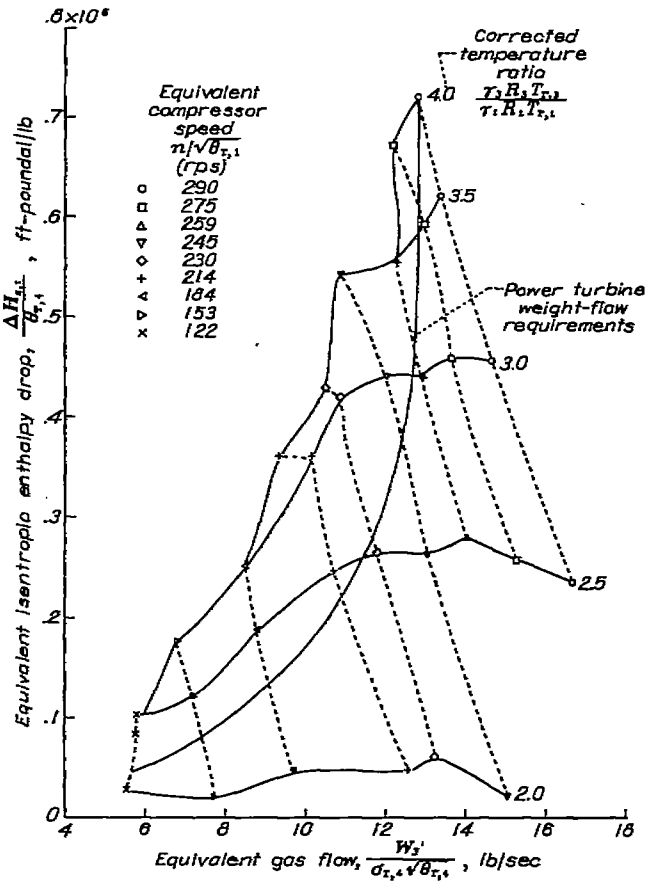

FIGURE 23.—Superposition of gas-generator and power-turbine characteristics.

of 0.87. The results of these computations are plotted in figure 24, which shows that the power turbine can develop 1800 horsepower (32.2×10^6 ft-poundal/sec) with a specific fuel consumption of 0.56 pound fuel per horsepower-hour at an equivalent compressor speed of 290 rps and a temperature ratio of 4.0 for the gas generator.

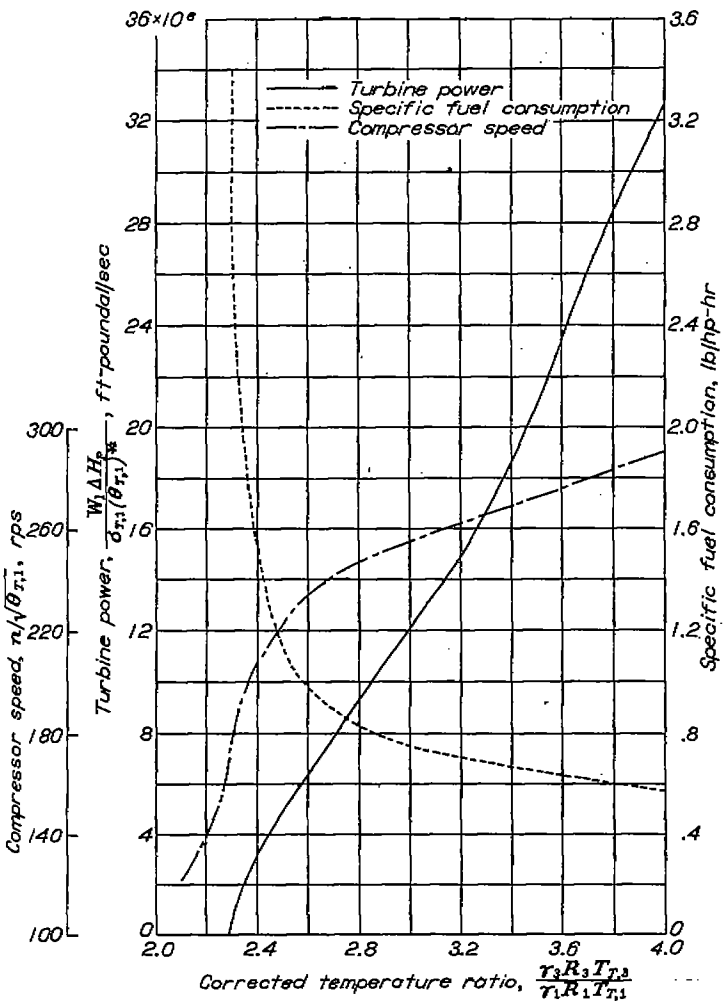

FIGURE 24.—Over-all performance characteristics of gas turbine.

The ineffectiveness of the engine at low speeds is shown by the fact that at a speed of 180 rps, which is 62 percent of the full speed, the power developed is only 3 percent of full power. This condition indicates difficulty in starting the engine but engine power increases rapidly with fuel input for temperature ratios more than 2.3. A slight decrease in specific fuel consumption from the values in figure 24 will be attained from the exhaust jet power because the pressure ratio of the nozzle is equal to the rampressure ratio. Inasmuch as the speed of the power turbine did not enter into the solution of this problem, the method of solution is always applicable for gas turbines whether or not the power turbine is connected with a gas-generator shaft, provided that the gas-flow pressure-ratio characteristics are independent of operating speed. If the turbine speed does influence the gas flow, the engine characteristics may be evaluated for each speed of the power turbine in the same manner as the example.

The operation of the compressor in this gas turbine is shown in figure 25 by the operating curve of the compressor. The operating curve approaches the surge line of the compressor at the highest speed, so that the performance curves of the gas turbine will show a decrease in engine power and efficiency as the speed and the temperature ratio increase over approximately 300 rps and approximately 4.2, respectively. There is no means in this case for obtaining higher output from the power turbine; however, additional engine power might be obtained at higher engine speeds and temperature ratio by bleeding some of the gas-generator discharge gas for application in a power jet or by redesigning the power turbine for a higher flow capacity.

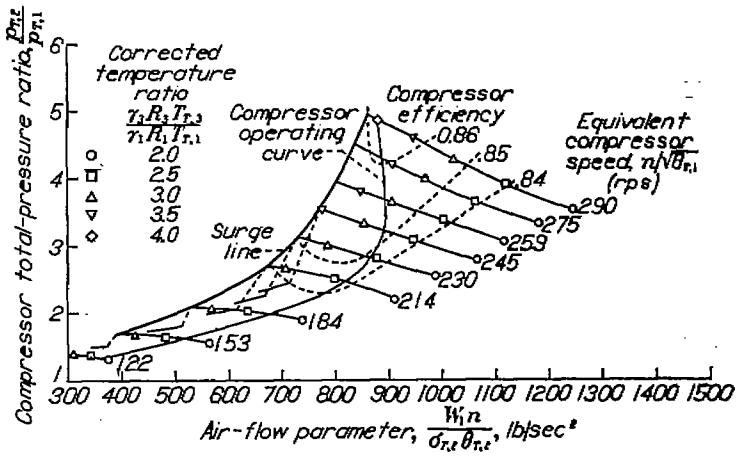

FIGURE 25.—Estimated compressor performance in gas-turbine engine.

SUMMARY OF RESULTS

The principal results of the experimental study of operation and interaction of the components of the turbojet engine and the influence of the components on over-all engine performance are summarized as follows:

1. The one-dimensional theory of combustion-chamber loss was inadequate to correlate the data obtained in the burner of the engine. This inadequacy was probably due to the simultaneous diffusion and burning in the combustion chamber of the engine.

2. The method of correlating combustion efficiency of the burner was adequate because the variables used correlated the data to curves that followed the expected trend in the practical range of combustion temperatures.

3. After corrections were made for tip leakage, the gas-flow pressure-ratio characteristics of the turbine obtained from cold-air component runs could be checked with the results obtained from the turbojet engine.

4. As predicted from the component test with cold air, the range of turbine characteristics obtainable from turbojet-engine experiments was insufficient to establish the turbine-efficiency characteristics or to indicate how the turbine operating conditions fit into these characteristics. Resetting of the compressor stator blades satisfactorily extended the range.

5. The efficiency contours obtained from engine data differed slightly from those obtained from component data. Although the peak efficiency in each case reached the same maximum value, in the component experiments this maximum occurred at a speed of approximately 180 rps, whereas in the engine experiments this maximum occurred at a speed of 155 rps.

6. Estimates of engine performance with realizable improvements in the bearings and the burners showed that improved matching of the compressor and turbine high-efficiency regions was attainable chiefly because of reduced bearing torque. The engine modifications resulted in improvements in engine performance of 5 and 15 percent in equivalent thrust and specific thrust, respectively, at 290 rps and temperature ratio of 3.0. At an equivalent speed of 290 rps and a temperature ratio of 4.0, the improvements were 9 and 21 percent in equivalent thrust and specific thrust, respectively. In some engines, improvement in component performance may possibly impair the matching of the components and result in no gain in over-all engine performance.

7. For engine acceleration, the operation points of the compressor for a fixed speed and temperature ratio were changed very little from steady-state operation but the turbine pressure ratio increased and the exhaust pressure ratio decreased from values for steady-state engine operation.

8. If the exhaust gases from the turbojet engine are used to drive a power turbine, a unit can be designed that will develop 1800 horsepower with a specific fuel consumption of 0.56 pound fuel per horsepower-hour at an equivalent compressor speed of 290 rps and a temperature ratio of 4.0 for the gas generator. Higher speeds and temperature ratios would result in a reduction of engine power and efficiency because of the low compressor efficiency for operation in the region of lower flow beyond the surge line.

CONCLUSIONS

The following generally valid conclusions can be drawn from this engine study:

1. A method of analysis has been developed for application to jet engines and gas-turbine engines, which clearly shows the operation of the compressor and turbine components under all conditions of engine operation and permits the estimation of the effect on engine performance of modifications in the performance characteristics of the engine components.

2. Approximate estimates of engine performance can be made from component calibration of the compressor and the turbine utilizing cold air. The accuracy of prediction of the gas-flow pressure-ratio characteristic with hot gas from cold-air calibration is quite good if proper clearance-flow corrections are made. If the turbine operates choked or nearly choked, the operation of the compressor in the engine may then be accurately predicted, but the value of the exhaust pressure ratio will reflect any inaccuracy in the turbine efficiency.

3. Complete evaluation of the turbine characteristics may not always be possible from experiments of the complete engine and elaboration of the experimental procedure may be necessary to extend the range of turbine operation.

4. The incidence of compressor surge during engine acceleration may be determined in the case of choked turbine flow from the operation point of the compressor for constant speed at the same temperature ratio and speed as for the beginning of acceleration. If the turbine is not choked, this criterion will be safe because the compressor in acceleration will operate at a condition slightly more removed from the surge line.

Flight Propulsion Research Laboratory,
National Advisory Committee for Aeronautics,
Cleveland, Ohio, *June 2, 1948.*

APPENDIX

SYMBOLS

The following symbols are used in this report:

$F_m(T_{T,3})$	clearance correction factor for turbine torque (or moment)
$F_g(T_{T,3})$	clearance correction factor for gas mass flow
f	fuel-air ratio
H	enthalpy, ft-poundal/lb
H_f	enthalpy of incoming fuel, ft-poundal/lb
h	heating value of fuel, ft-poundal/lb
n	rotative speed of engine, rps
P_a	auxiliary power consumption such as bearing loss, ft-poundal/sec
p	gas pressure, lb/sq ft
R	gas constant, ft-poundal/(lb)(°R)
T	gas temperature, °R
W	mass flow of gas, lb/sec
W_3'	mass flow of gas through turbine corrected for turbine-blade-tip leakage, lb/sec
γ	ratio of specific heats of gas, c_p/c_v
ΔH_c	stagnation enthalpy rise of air in compressor, $H_{T,2}-H_{T,1}$, ft-poundal/lb
ΔH_p	stagnation enthalpy drop of gas in power turbine, ft-poundal/lb
$\Delta H_{s,c}$	isentropic rise in stagnation enthalpy of gas in compressor, ft-poundal/lb
$\Delta H_{s,t}$	isentropic drop in stagnation enthalpy of gas in turbine, ft-poundal/lb
ΔH_t	stagnation enthalpy drop of gas in turbine, ft-poundal/lb
$\Delta H_t'$	stagnation enthalpy drop of gas in turbine corrected for turbine-blade-tip leakage, ft-poundal/lb
η	combustion efficiency
θ	ratio of square of sonic speed of gas to square of sonic speed for normal air
ρ	gas density, lb/cu ft
σ	ratio of gas density to normal air density, ρ/ρ_{st}

Subscripts:

0	free-stream
1	compressor inlet
2	compressor outlet
3	turbine inlet
4	turbine outlet
st	standard air
T	stagnation or total

REFERENCES

1. Sinnette, John T., Jr., Schey, Oscar W., and King, J. Austin: Performance of NACA Eight-Stage Axial-Flow Compressor Designed on the Basis of Airfoil Theory. NACA Rep. 758, 1943.
2. Sinnette, John T., Jr., and Voss, William J.: Extension of Useful Operating Range of Axial-Flow Compressors by Use of Adjustable Stator Blades. NACA Rep. 915, 1948.
3. King, J. Austin, and Regan, Owen W.: Performance of NACA Eight-Stage Axial-Flow Compressor at Simulated Altitudes. NACA ACR E4L21, 1944.
4. Goldstein, Arthur W.: Analysis of Performance of Jet Engine from Characteristics of Components. I—Aerodynamic and Matching Characteristics of Turbine Component Determined with Cold Air. NACA Rep. 878, 1947.
5. Keenan, Joseph H., and Kaye, Joseph: Thermodynamic Properties of Air. John Wiley & Sons, Inc., 1945.
6. Pinkel, Benjamin, and Turner, L. Richard: Thermodynamic Data for the Computation of the Performance of Exhaust-Gas Turbines. NACA ARR 4B25, 1944.
7. Stodola, A.: Steam and Gas Turbines. Vol. II. McGraw-Hill Book Co., Inc., 1927, p. 271. (Reprinted, Peter Smith (New York), 1945.)
8. Pinkel, I. Irving, and Shames, Harold: Analysis of Jet-Propulsion Engine Combustion-Chamber Pressure Losses. NACA Rep. 880, 1947.
9. McLellan, Charles H., and Nichols, Mark R.: An Investigation of Diffuser-Resistance Combinations in Duct Systems. NACA ARR, Feb. 1942.